Lightning-Fast Convective Outlooks: Predicting Severe Convective Environments with Global AI-based Weather Models

Monika Feldmann[1], Tom Beucler[2], Milton Gomez[2], Olivia Martius[1]

[1]Institute of Geography - Oeschger Centre for Climate Change Research, University of Bern
[2]Faculty of Geosciences and Environment - Expertise Center for Climate Extremes, University of Lausanne

arXiv:2406.09474v2 [physics.ao-ph] 9 Sep 2024

Key Points:

- AI-based global weather models produce forecasts with sufficient accuracy to derive instability and shear metrics skillfully
- The best AI-based weather models are capable of competing with state-of-the-art numerical weather predictions of instability and shear
- This is a major step towards computationally inexpensive and fast convective outlooks

Corresponding author: Monika Feldmann, monika.feldmann@unibe.ch

Abstract

Severe convective storms are among the most dangerous weather phenomena and accurate forecasts mitigate their impacts. The recently released suite of AI-based weather models produces medium-range forecasts within seconds, with a skill similar to state-of-the-art operational forecasts for variables on single levels. However, predicting severe thunderstorm environments requires accurate combinations of dynamic and thermodynamic variables and the vertical structure of the atmosphere. Advancing the assessment of AI-models towards process-based evaluations lays the foundation for hazard-driven applications. We assess the forecast skill of three top-performing AI-models for convective parameters at lead-times of up to 10 days against reanalysis and ECMWF's operational numerical weather prediction model IFS. In a case study and seasonal analyses, we see the best performance by GraphCast and Pangu-Weather: these models match or even exceed the performance of IFS for instability and shear. This opens opportunities for fast and inexpensive predictions of severe weather environments.

Plain Language Summary

Over the past year, several global AI-based weather models were released and produce a similar quality of forecasts as traditional weather models. AI-models are very fast and computationally cheap to produce forecasts. The evaluation of AI-models has largely focused on single atmospheric variables at certain heights. To forecast specific phenomena, such as thunderstorms, a combination of variables must be accurate at multiple heights. Here we use the output of AI-models to derive thunderstorm-related parameters. We compare 10-day-forecasts between 3 AI-models and a state-of-the-art traditional weather model while using a reanalysis dataset as the reference.

With the example of a tornado outbreak in the southern United States, we see that all models are capable of forecasting thunderstorm parameters multiple days in advance. To obtain a robust assessment, we evaluate the entire thunderstorm season in 2020 in regions such as North America, Europe, Argentina, and Australia, where severe thunderstorms occur frequently. Two of the three AI-models achieve similar or even better results than the traditional weather model while being much cheaper to operate computationally.

Forecasting thunderstorm parameters directly, instead of calculating them afterwards, is likely to produce even better results. This opens opportunities for rapid and accessible forecasts for severe thunderstorm phenomena.

1 Introduction

Artificial intelligence (AI)-based deterministic forecasts are revolutionizing the landscape of medium-range weather forecasting (Ebert-Uphoff & Hilburn, 2023; Bouallègue et al., 2024). Among the models released in the past year are FourCastNet (Bonev et al., 2023), GraphCast (Lam et al., 2023) and Pangu-Weather (Bi et al., 2023). They are capable of forecasting the main atmospheric state variables on various pressure levels within seconds (on GPU, Wong, 2023), with a skill similar to the deterministic IFS model (Integrated Forecasting System, Bougeault et al., 2010, operational version of IFS) of the ECMWF (European Centre for Medium-range Weather Forecasts). AI-based weather predictions are rapidly revolutionizing weather forecasting (Bouallègue et al., 2024; Olivetti & Messori, 2024a; Beucler, Koch, et al., 2024; Brunet et al., 2023; Govett et al., 2024; McGovern et al., 2024) with scientists and forecasting centers calling for action to scrutinize AI-model performance from various perspectives, going beyond simply verifying the atmospheric state (Ebert-Uphoff & Hilburn, 2023; Jeppesen, 2024; Bonavita, 2024). First studies investigate the robustness of forecasts for extremes (Charlton-Perez et al., 2024; Olivetti & Messori, 2024b) and model behavior in idealized experiments (Hakim & Masanam, 2024).

We focus on the specific, application-oriented task of accurately predicting atmospheric profiles in convective environments. The skillful prediction of convective environments requires high accuracy in the vertical profile and the simultaneous, correct prediction of both thermodynamic (temperature and humidity) and kinematic components (vertical wind shear). Convective storms require instability, governed by the vertical temperature and moisture profile (e.g., Houze, 2014; Trapp, 2013). Severity is modulated by wind shear, emphasizing the importance of the wind profile (Houze, 2014; Trapp, 2013). By combining instability and wind shear, severe convective environments, that are related to particularly hazardous and impactful thunderstorms, can be identified (e.g., Taszarek et al., 2020; Kunz, 2007; H. E. Brooks et al., 2003).
Severe thunderstorms are among the most hazardous weather phenomena and caused substantial losses worldwide in recent years (e.g., Bowen et al., 2024). Severe thunderstorms can produce large hail and severe wind gusts, along with torrential rain, lightning strikes, and tornadoes (Houze, 2014; Markowski & Richardson, 2010).
Global AI-models at medium-range lead-times currently provide weather information on a 0.25° grid. These models can hence not explicitly forecast severe storms. Therefore we focus on verifying pre-convective environments, characterized by mesoscale patterns of instability and wind shear. These environments provide information on the propensity of the atmosphere to produce severe storms (e.g., Taszarek et al., 2021, 2020; H. E. Brooks, 2013) and are used to forecast severe convection (Battaglioli et al., 2023; H. Brooks et al., 2011; Kunz, 2007). Accurate and inexpensive forecasts of mesoscale convective environments enable the timely assessment of severe convective outlooks for hazardous weather warnings.

2 Data

We focus our analysis on the year 2020, which is established as a reference year in the benchmark dataset "Weatherbench2" (Rasp et al., 2024) and was not used in training AI-models. We evaluate the three AI-models Pangu-Weather (Bi et al., 2023), GraphCast (Lam et al., 2023), and FourCastNet (Bonev et al., 2023). We selected models with publicly accessible code and a stable version. Other AI-based global models have been developed (AIFS, FuXi, Aurora and ClimaX; Lang et al., 2024; Chen et al., 2023; Bodnar et al., 2024; Nguyen et al., 2023), but do not meet our evaluation requirements. The models are compared with the performance of the deterministic IFS-HRES (Haiden et al., 2019, IFS cycle 46r1). The reference model IFS is the operational, physics-based, numerical weather prediction model at ECMWF, used for global medium-range forecasts (Thepaut & Courtier, 1991; Bougeault et al., 2010). The ERA-5 reanalysis (Hersbach et al., 2020) serves as a ground truth. We obtain Pangu-Weather, GraphCast, and IFS data through "Weatherbench2" (Rasp et al., 2024). FourCastNet forecasts are produced with the "ai-models" code-release of ECMWF (ECMWF, 2023).
In terms of architecture, Pangu-Weather is a transformer model that uses a 3-D visual earth transformer to encode the relative location on a sphere and additionally employs a hierarchical temporal aggregation, combining a 24h-prediction model with a 6h-prediction model (Bi et al., 2023). GraphCast is a graph neural network, which is particularly useful for spatially structured data, and uses successive 6h-predictions (Lam et al., 2023). "FourCastNet v2 small" is a transformer model, employing spherical Fourier neural operators (SFNO) to account for the spatial encoding of a sphere (Bonev et al., 2023).
All data is gridded at a 0.25° resolution, and IFS' native 0.125° resolution is regridded using the MIR method (Meteorological Interpolation and Regridding, Barratt, 2017). The forecasts are available twice daily at 00h UTC and 12h UTC up to 10 days lead-time in 6-hour increments. The AI-models are initialized from both ERA-5 and the IFS analysis. This reflects the conditions they were trained in (ERA-5) compared to an operational prediction set-up (IFS analysis). GraphCast has an additional operational version specifically tuned to being initialized with IFS data (GraphCast-oper). IFS is initialized with the IFS analysis.

For the computation of convective parameters, we use the temperature (T), specific humidity (Q), geopotential, and horizontal wind on the surface and pressure levels listed in Table S1 (see Section 3.1). The models differ in the available pressure levels and in the moisture variable that they predict, with most models providing 13 pressure levels between 50 and 1000 hPa and predicting Q. FourCastNet predicts relative humidity (RH), which needs to be converted to Q before deriving CAPE. An overview is provided in Table S1.

3 Methods

3.1 Deriving convective parameters

We focus on the following convective parameters: convective available potential energy (CAPE), deep-layer shear (DLS), and a combined parameter of both called wmax-shear (WMS). CAPE is derived with the implementation for most unstable CAPE found in WRF-python (Ladwig, 2017), which launches a parcel profile above the surface at the height of highest equivalent potential temperature, using temperature, moisture, and geopotential at pressure levels, as well as surface elevation, pressure, and temperature. The relatively coarse vertical resolution reduces the accuracy of the CAPE calculation (Wang et al., 2021; Mensch, 2021). However, we apply the same procedure to all datasets, hence treating them equally. We thereby artificially reduce the number of vertical levels available in the IFS and ERA-5 data. To approximate DLS, we compute the magnitude of the differential wind vector between the 10 m and the 500 hPa level. Further details on the computation of convective parameters are described in Text S1.

3.2 Forecast evaluation

To evaluate the forecast quality, we use several different scores. We first compute the root mean square error (RMSE) and the bias, two standard scores. To account for displacement errors and avoid the so-called 'double penalty' (Gilleland et al., 2009; Gilleland, 2013), we additionally use the fractional skill score (FSS, Mittermaier, 2021) and the structure, amplitude, and location (SAL) score, which evaluates these three properties individually (Wernli et al., 2008, 2009). Additional information on the interpretation of the scores is provided in Table S2.

We compute the FSS for two thresholds for each variable (300 and 1000 J kg^{-1} CAPE; 300 and 500 m^2 s^{-2} WMS, Taszarek et al., 2017), with a neighborhood size of 1°, oriented on the gradients between categories of convective outlooks. The SAL is computed for 300 J kg^{-1} CAPE, describing the convective environment. While the thresholds also include environments with only a moderate likelihood of convective storm formation, they serve as an estimated lower bound on severe convective storm occurrence.

4 Case Study: US tornado outbreak

4.1 Synoptic situation

Throughout 12 and 13 April 2020, 141 tornadoes were reported in 10 states, ranging up to a strength of EF4 (Storm Prediction Center, 2020a, 2020b). With an estimated 450 Million US$ worth of property damage and 38 fatalities, this tornado outbreak was among the highest-impact events in the southern states (Beddoes, 2020), contributing to 2020 having the highest severe convective storm damages in the past (Bevere & Weigel, 2021).
The tornado outbreak was characterized by an anomalously warm period in the preceding month (Copernicus Services, 2020), leading to high sea surface temperatures in the Gulf of Mexico. The convective period was induced by a deep trough moving across the US. In the warm sector, warm and moist air from the Gulf was advected over the South-

eastern states. Simultaneously, the approaching trough was associated with high DLS, which is crucial for convective organization. The convective potential of the situation was well forecast, the storm prediction center issued the first warnings four days ahead (Dean & Dial, 2020).

While this event was most striking because of the large number of tornadoes, we focus on the convective environment characterized by CAPE and DLS. Figure 1 shows the evolution of pressure-level CAPE, DLS, the 500 hPa geopotential height anomaly, and the surface temperature anomaly from ERA-5 during the outbreak.

The in-depth analysis of model forecast performance will focus on 12 April 2020 at 12:00 UTC, a few hours before the most intense storms occurred.

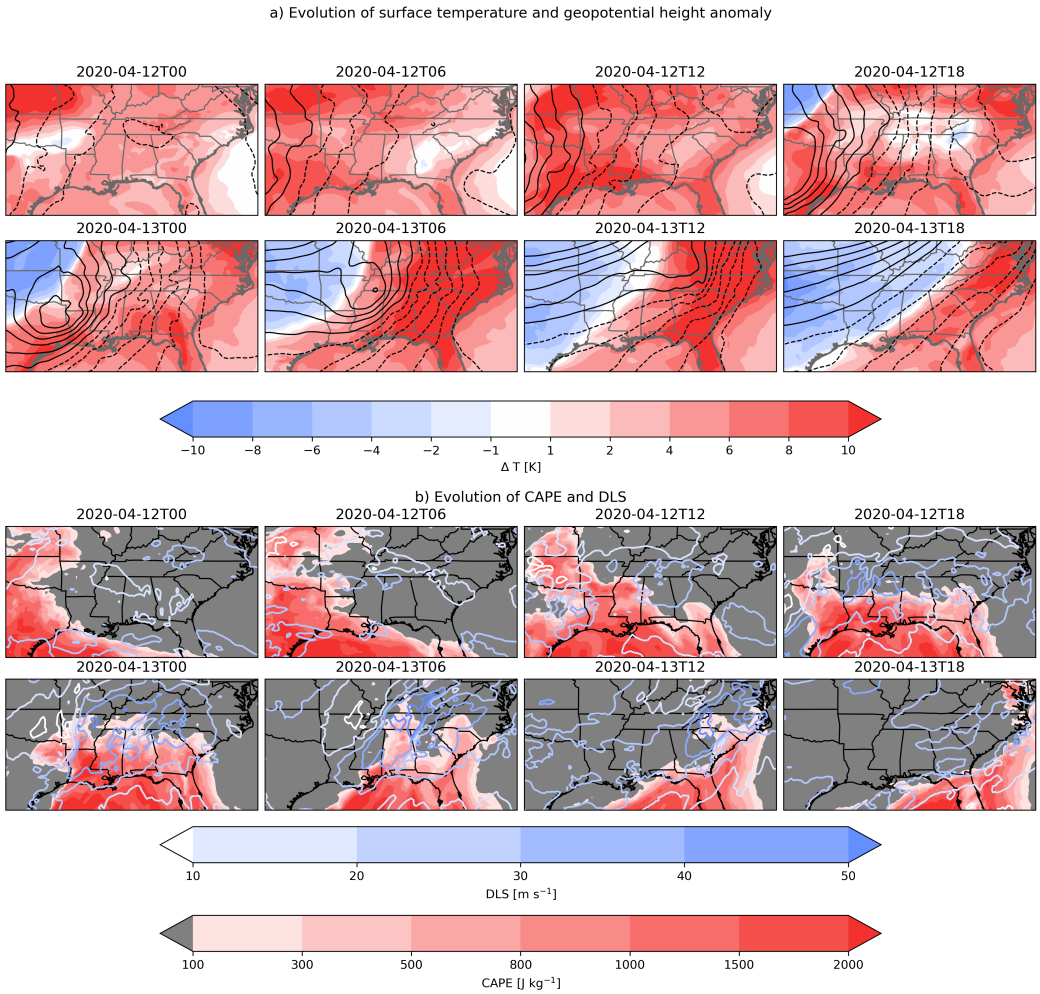


Figure 1. Synoptic situation in ERA-5 on April 12 and 13 2020, showing a deep trough moving across the United States, with anomalously warm temperatures and high CAPE values in the warm sector; a) Climatological geopotential height anomaly and surface temperature anomaly, contours indicate positive (dashed) and negative (solid) anomalies of geopotential height in 20 m increments b) pressure-level-derived CAPE and DLS, hatched area indicates where DLS >20 m s^{-1}.

4.2 Forecasting CAPE and DLS

We established CAPE from ERA-5 pressure levels as the reference. However, to assess realistic convective outlooks, we additionally compare this to CAPE derived from model levels and soundings. Figure 2A) shows a comparison of both (Fig. 2a,b) and their density distribution over the entire case duration (Fig. 2c). They correlate well (R^2=0.79), however, the distribution is narrowed, with an overestimation of low values and an underestimation of high values. When comparing to soundings (Fig. 2d), any ERA-5 derived CAPE generally tends to be underestimated with respect to the radio-sounding. Diagrams of the observed soundings and ERA-5-modeled pseudo-soundings are provided in Fig. S1.
We first determine whether AI-models overall produce realistic CAPE and DLS values at a short lead-time of 12 hours. Fig. 2B) shows all models initialized with IFS analysis (Fig. 2e-h, absolute and difference to ERA-5). All models produce CAPE values in the right order of magnitude with a spatial distribution of DLS that corresponds well to the reference. Nonetheless, we can see differences between the models. All AI-model fields appear smoother than the reference data. IFS has the highest degree of spatial detail in both DLS and CAPE, while the AI-models mostly capture the larger-scale features. The high degree of detail in IFS, however, is penalized in the standard performance scores, as already a small displacement of features can lead to increases in RMSE (Fig. 2e, RMSE-IFS=312 J kg^{-1}, RMSE-GraphCast-oper=271 J kg^{-1}; for all scores see Table S4). FourCastNet-oper underestimates CAPE in this case (Fig. 2h). Of the AI-models, GraphCast-oper shows the closest match in terms of location and magnitude to ERA-5 (Fig. 2h).

We next inspect the lead-time 156 hours / 6.5 days (Fig. 2C). At this longer lead-time, IFS displaces the event eastwards (Fig. 2i), however, the magnitude of CAPE values is correct. This leads to large absolute errors (RMSE-IFS 829 J kg^{-1}). Pangu-Weather-oper's forecast also suffers from displacement error, owed to a very different spatial structure of the event (Fig. 2j, RMSE-PanguWeather-oper 570 J kg^{-1}). GraphCast-oper has the best agreement in terms of event structure and location (Fig. 2k, RMSE-GraphCast-oper 520 J kg^{-1}). FourCastNet-oper strongly underestimates CAPE and also has the largest degree of smoothing (Fig. 2l). It misses most land areas that experience high CAPE and DLS. Nonetheless, we highlight here, that all models capture an area of elevated CAPE values more than 6 days in advance, in co-location with high DLS.

5 Seasonal and regional analyses

To investigate performance scores, we derive CAPE and WMS for North America, Europe, Argentina, and Australia and their respective convective seasons. CAPE and WMS are filtered by a land-sea-mask to focus on convectively relevant areas. Table S3 summarizes the regions' extent and seasons. We then compute the lead-time-dependent scores for each model.

5.1 The North American convective season

Figure 3 depicts the lead-time-dependent scores throughout the entire convective season for the USA. We include here both the models initialized with ERA-5 and with IFS analysis, initialized at 00 UTC.

The RMSE of CAPE (Fig. 3a) shows close proximity of the scores of Pangu-Weather, GraphCast, and IFS. They lie well within each other's interquartile range (IQR). FourCastNet is a notable exception, performing consistently worse than all other models. GraphCast and Pangu-Weather tend to outperform IFS slightly. Since they are optimized on RMSE (albeit on different variables), we expect them to perform best in this metric. The BIAS (Fig. 3b) shows more diversity, with IFS having an increasingly positive BIAS and Pangu-Weather a quite stationary BIAS, centered on 0. GraphCast moderately under-

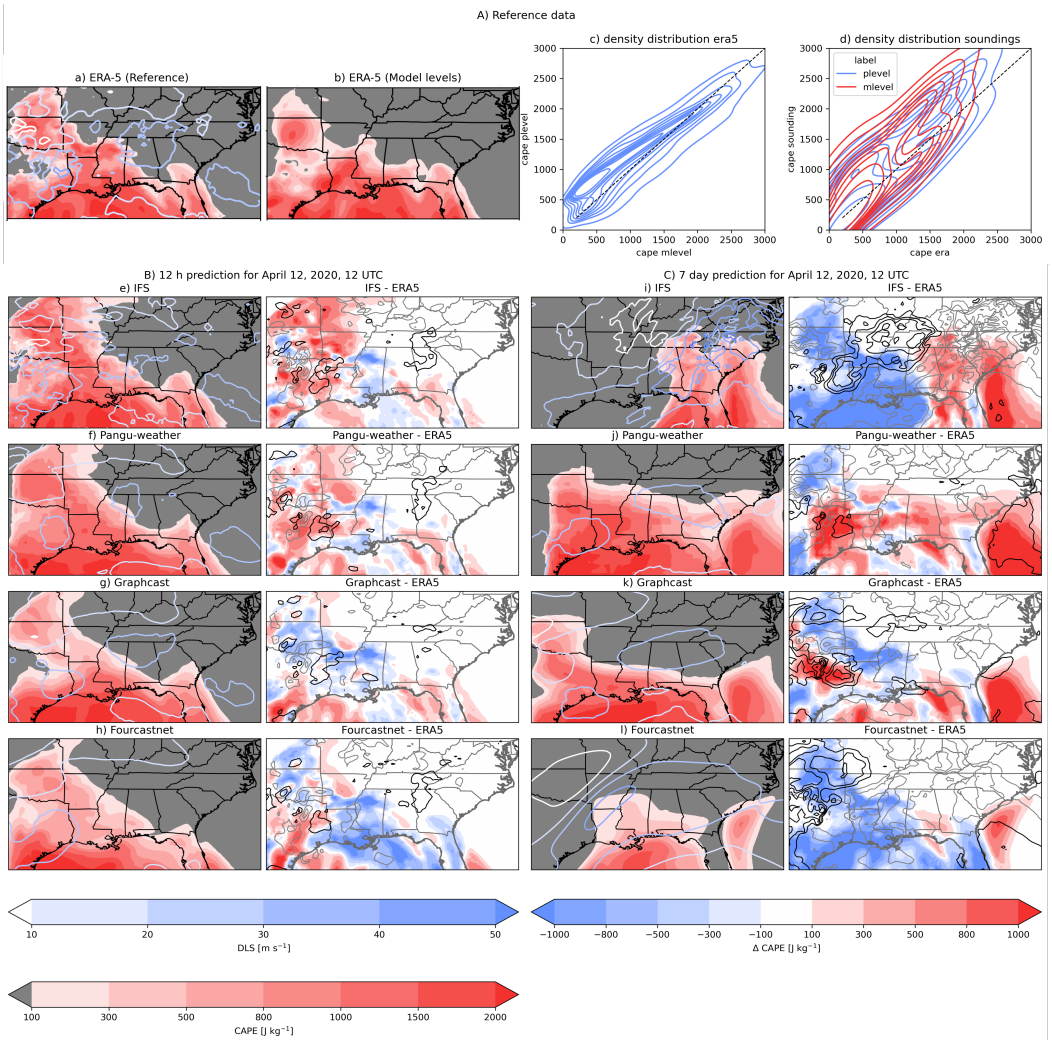


Figure 2. Forecast comparison of CAPE and DLS at 12h and 6.5 days lead-time; A) ERA-5 data of CAPE and DLS on April 12, 2020 at 12 UTC; a) CAPE and DLS from pressure levels, b) CAPE from model levels, c) density diagram of CAPE from pressure and model levels, d) density diagram of CAPE from pressure and model levels against observed soundings. A) 12h forecast of CAPE and DLS in comparison to ERA5 (e-h) B) 6.5-day day forecast of CAPE and DLS in comparison to ERA5 (i-l); contours indicated positive (gray) and negative (black) areas of Δ DLS in 5 m s^{-1} increments

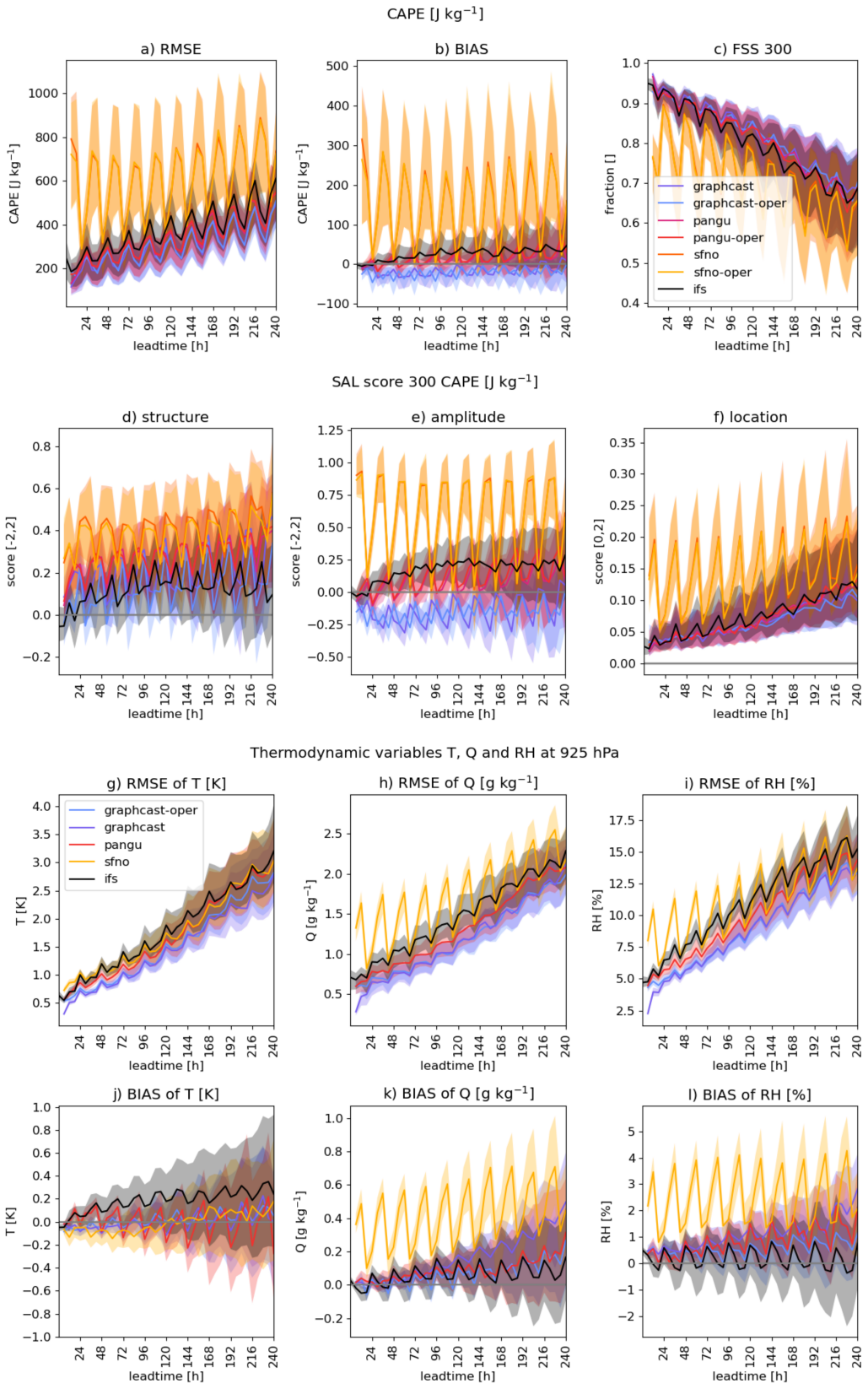


Figure 3. Seasonal evaluation of CAPE for North America at 00 UTC initialization shows Pangu-Weather and GraphCast outperforming IFS, with a moisture bias impacting the performance of FourCastNet. Top row: a) RMSE, b) BIAS, c) FSS_{300}; Second row: SAL components for CAPE >300 J kg^{-1}; color legend in panel c); Third row: RMSE of T, Q and RH at 925 hPa (g-i); Fourth row: BIAS (j-l); model legend in panel g). Solid line depicts the median and shading the interquartile range.

estimates CAPE, while FourCastNet strongly overestimates CAPE, contrasting with the underestimation in the case study. The seasonal analysis is dominated by the principal convective season in the Great Plains, whereas the case study focuses on a spring convective event in the Southeast. For the FSS_{300} (Fig. 3c), GraphCast and Pangu-Weather are slightly better than IFS at intermediate lead-times. FourCastNet is consistently worse, largely lying outside of the IQR of the other models. In terms of SAL scores, the amplitude score mirrors the BIAS (Fig. 3b,e). The positive structure score shows the smoother behavior of the AI-models (Fig. 3d). It is important to note, that structure, amplitude, and location are not wholly independent of one another, as strong biases also affect structure and location of objects. The location score shows the largest dependence on lead-time, steadily increasing (Fig. 3f). Overall IFS scores close to '0' in both structure and amplitude, while the location score shows the strongest deterioration over lead-time. A clear pattern visible in all models is a regular spikiness on a 24-hour frequency, when separating the data into the 00 UTC (Fig. 3) and 12 UTC (SI Fig. S2) initializations. This is owed to the strong diurnal cycle of CAPE, which depends on the diurnal cycle of temperature (Leon, 2018; Lawson & Gallus Jr, 2016) and humidity. The models tend to perform better at night and in the early morning when CAPE is naturally low. The errors are higher during the day and in the evening when peak CAPE values occur. For Pangu-Weather this additionally coincides with the change between the 6h- and 24h-integration models, leading to a 24h cycle of skill even in combined initialization times (see Fig. 4).

Given the similarity between the initializations with ERA5 and IFS analysis, we focus the next analyses on the initializations with IFS (previously flagged as "oper"), mimicking an operational context. Since GraphCast (initialized with ERA-5) and GraphCast-oper (initialized with IFS) are two different model versions, we maintain both.

5.2 The impact of thermodynamic conversions

With FourCastNet being an outlier, one core difference is the prediction of RH instead of Q. Q is used most commonly, but due to the relatively strong boundedness, RH has been shown to generalize better in some machine learning applications (Beucler, Gentine, et al., 2024; Lin et al., 2024). This mostly applies to large domain shifts under climate change, where Q is no longer well-constrained. At the weather timescale, Q can be assumed to be in a stable value range. To calculate CAPE, RH needs to be converted to Q. The conversion is dependent on the temperature and pressure, making this an additional processing step, where forecast errors can compound. To quantify this effect, we additionally compare all models' RMSE and BIAS for RH, Q, and T in Figure 3. The RMSE (Fig. 3g) and BIAS (Fig. 3j) of T are quite similar across all models, indicating that the large differences in CAPE are not primarily owed to T. At short lead-times FourCastNet performs only marginally worse. Looking at Q, it becomes evident that FourCastNet not only has a larger RMSE (Fig. 3h) but also consistently overestimates Q (Fig. 3k), which does not improve much at short lead-times. For RH it becomes evident, that despite this being the natively predicted variable, FourCastNet also does not perform particularly well. The BIAS (Fig. 3l) remains consistently positive. GraphCast-oper and Pangu-Weather consistently have a lower RMSE and BIAS (Fig. 3i,l), despite RH being a converted variable in their output. Consequently, FourCastNet suffers from a double penalty - the moderately good RH undergoes further conversion to Q before being integrated into the computation of CAPE. Moisture is a key component in determining the lifting condensation level, which strongly impacts the integral of CAPE, leading to large compounding errors.

5.3 Global convective hotspots

We next compare the models' performance in additional convectively active regions: Europe, Argentina, and Australia. Figure 4 depicts the RMSE, BIAS, and FSS_{300} for

CAPE, and the FSS_{300} for WMS, computed on both the 00 UTC and 12 UTC initializations.

At first glance, the RMSE is highest in North America and Argentina (Fig. 4a and i). This is partly due to the overall magnitude of CAPE values during the 2020 convective seasons; a value of 300 J kg^{-1} falls at the 84th and 86th percentiles of the CAPE distribution in these regions, compared to the 90th and 93rd percentiles in Australia and Europe, respectively. The magnitude of CAPE impacts the FSS_{300}, as the FSS generally decreases as the threshold approaches the tail end of the overall value distribution. Hence it is consistent that the FSS_{300} is overall best in North America (Fig. 4c). FourCastNet generally performs worse and has a wider range of performance scores than the other models. This is primarily driven by the quality of its RH forecast. Australia is an exception, where FourCastNet achieves similar RMSE (Fig. 4m) to the other models, albeit with a very large IQR. The lower RMSE of CAPE stems from a better prediction of RH in this region (figure not shown).
In all regions, GraphCast-oper and GraphCast show the lowest RMSE of CAPE (Fig. 4a,e,i,m) and over most lead-times the highest FSS_{300} (Fig. 4c,g,k,o), followed by Pangu-Weather and IFS. Despite the small differences, the high consistency across multiple regions shows this as systematic behavior.
The FSS_{300} of CAPE and FSS_{500} of WMS show similar behavior, with the WMS achieving lower scores, being at a higher convective threshold. This indicates that skill is primarily driven by CAPE, while shear plays a minor role in the predictability of convective environments. Both FSS show very similar performance for GraphCast, Pangu-Weather, and IFS. There is no consistent ranking as in the RMSE, highlighting the importance of considering multiple performance scores.

6 Discussion and Conclusion

As shown in Section 5, Pangu-Weather, GraphCast-oper, and GraphCast are capable of producing realistic forecasts of the mesoscale convective environment at medium-range lead-times in a matter of minutes and perform similarly to IFS. FourCastNet has the strongest deficiencies, partially owed to the additional processing step from RH to Q. However, as Section 5.2 shows, forecasting errors in convective parameters are also owed to overall issues in forecasting moisture. With GraphCast and Pangu-Weather providing reasonable RH values derived from Q, we conclude that RH is not necessarily a worse choice than Q, but rather that "FourCastNet v2 small" specifically has issues in forecasting moisture. The best choice in moisture variable depends on the application, as every thermodynamic conversion in a non-physical model comes with additional uncertainty.
The evaluation of different regions shows the global capability of Pangu-Weather and GraphCast. Despite regional performance differences, the ranking of models remains stable, with GraphCast consistently performing best in terms of RMSE, followed by Pangu-Weather, and IFS. These models score very similarly, and their systematic differences are smaller than the uncertainty of the initialization. For the FSS, Pangu-Weather and GraphCast are able to achieve similar scores to IFS, but do not consistently outperform it. This highlights how the RMSE, which is used in model training, is an incomplete perspective on model performance.
The perceived discrepancy between the case study and the evaluation of the North American convective season shows how case studies can be misleading for performance evaluation. The case study takes place in spring in the Southeastern States, while the bulk of the convective season is driven by the Great Plains in summer. Particularly the moderately good performance of FourCastNet in this instance is not typical when over most of the summer season, RH and subsequently CAPE are largely overestimated. An additional example case during the summer is provided in Figure S2. This highlights the necessity to evaluate a larger sample of cases, before drawing conclusions on AI-model-

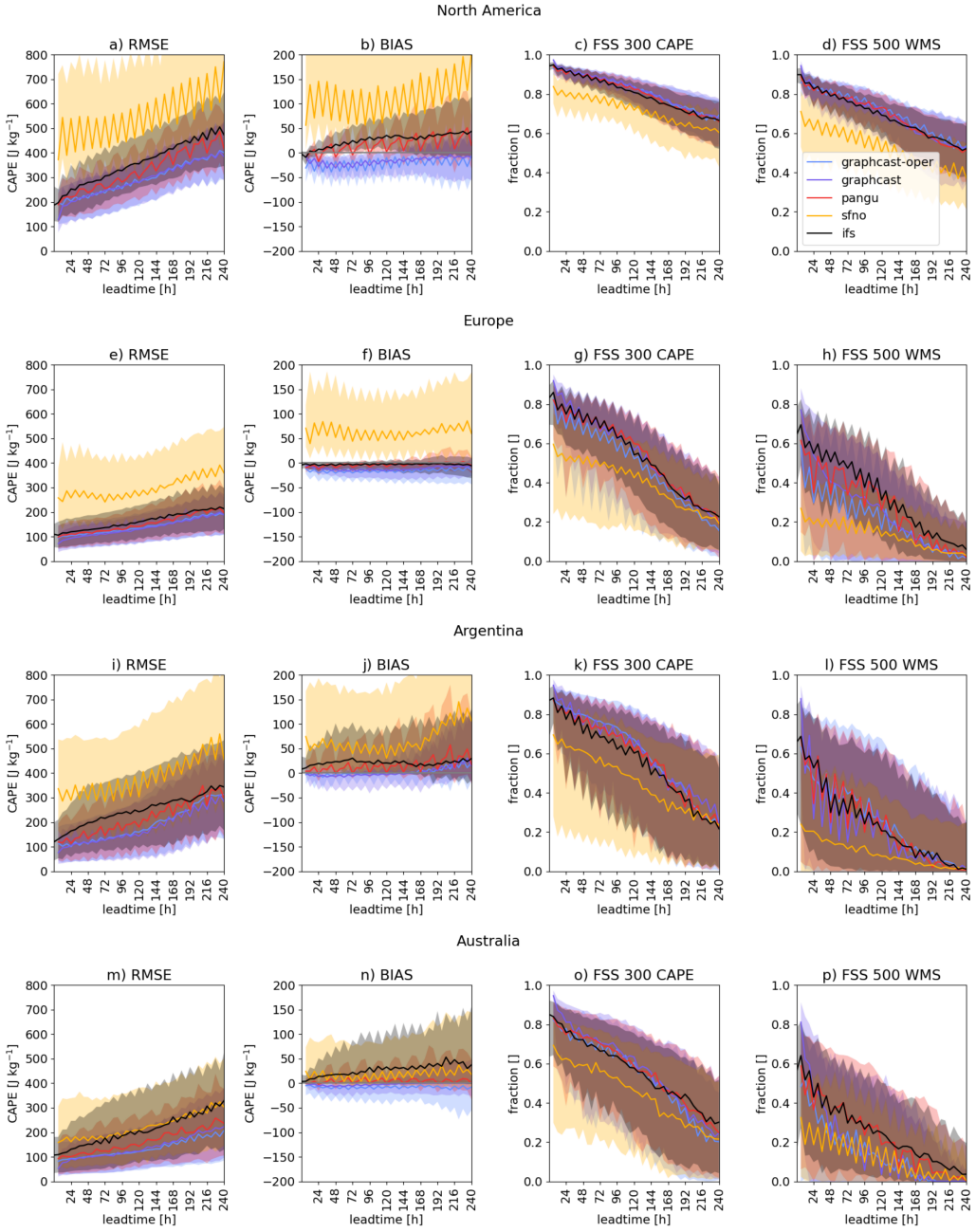


Figure 4. Seasonal evaluation of CAPE in North America (Apr-Aug, a-d), Europe (Apr-Sep, e-h), Argentina (Sep-Feb, i-l) and Australia (Sep-Feb, m-p) shows good performance of Graph-Cast and Pangu-Weather; solid line depicts median of score, the IQR is shown in shading

performance. While a single convective season is still rather short, the consistency of the results across four different global regions indicates robustness in our evaluation.
Despite the shortcomings of deriving CAPE from vertically coarse pressure levels, the promising results of GraphCast and Pangu-Weather indicate that CAPE is a worthwhile prediction variable. Predicting CAPE directly by training on ERA-5's model-level CAPE instead of deriving it, would likely be the most skillful approach. For instance, foundation models are designed for easier addition of variables after the main training of the model.
While forecasting convective environments is a large step closer to application-oriented forecasting, it still lacks the specificity of impact-oriented hazard predictions. Rapid progress in downscaling through super-resolution may enable direct hazard forecasts in the foreseeable future.
Currently, the vertical coarseness limits the number of convectively relevant variables that can be derived. We refrained from evaluating convective inhibition, near-surface shear, or helicity due to the limited resolution. However, these are key metrics for assessing convective initiation and convective hazards, especially tornadoes. With forecasters exploiting a myriad of convective parameters, it remains to be seen how practicable the direct prediction of additional convective parameters is in contrast to increasing the vertical resolution.
Taking this first step of deriving CAPE and DLS in AI-models already provides useful information for severe convective outlooks, which are key for severe weather warnings. This highlights how application-oriented products can be derived from AI-generated forecasts, with similar skill to operational numerical models. Especially with their very short runtime, they can deliver very timely forecasts at a low computational cost. This step towards process-based assessment of AI-models is crucial for the future development of hazard-driven applications.

Open Research Section

The IFS, ERA-5, Pangu-Weather, and GraphCast data were accessed through "Weatherbench2" (Rasp et al., 2024). FourCastNet predictions were computed with the code release of ECMWF (ECMWF, 2023). The code used to process the forecast data and produce the visualizations can be accessed at `https://github.com/feldmann-m/AI-storm` with the assigned DOI `https://doi.org/10.5281/zenodo.12527391`.

Competing interests

MF and OM are in positions funded by the Mobiliar Insurance Group. This funding source played no role in any part of the study.

Acknowledgments

We thank Zied Ben Bouallegue and Matthew Chantry for insightful discussions on the current state of AI-weather-forecasting. We also thank Louis Poulain-Auzéau for his work on installing the AI-models.
OM acknowledges support from the Swiss National Science Foundation project No. CRSII5_201792.
MF processed the data, created the visualizations, and wrote the manuscript. TB provided computational resources and expertise on the properties of AI-models and their evaluation. MG produced the FourCastNet predictions, assisted with computational aspects, and provided valuable expertise. OM co-designed the project and advised it. All authors reviewed the manuscript.

References

Barratt, M. (2017, August). The new ECMWF interpolation package MIR [Text]. *ECMWF*. Retrieved 2024-06-03, from https://www.ecmwf.int/en/newsletter/152/computing/new-ecmwf-interpolation-package-mir doi: 10.21957/h20rz8

Battaglioli, F., Groenemeijer, P., Tsonevsky, I., & Púčik, T. (2023). Forecasting large hail and lightning using additive logistic regression models and the ecmwf reforecasts. *Natural Hazards and Earth System Sciences*, *23*(12), 3651–3669. Retrieved from https://nhess.copernicus.org/articles/23/3651/2023/ doi: 10.5194/nhess-23-3651-2023

Beddoes, B. (2020). *Ranking the easter 2020 tornado outbreak versus the worst outbreaks in history; accessed on 2024-05-28.* Retrieved from https://www.whsv.com/content/news/Ranking-the-Easter-2020-outbreak-versus-the-worst-outbreaks-in-history-569861941.html

Beucler, T., Gentine, P., Yuval, J., Gupta, A., Peng, L., Lin, J., ... Pritchard, M. (2024, February). Climate-invariant machine learning. *Science Advances*, *10*(6). Retrieved 2024-04-04, from https://www.science.org/doi/full/10.1126/sciadv.adj7250 doi: 10.1126/sciadv.adj7250

Beucler, T., Koch, E., Kotlarski, S., Leutwyler, D., Michel, A., & Koh, J. (2024). Next-generation earth system models: Towards reliable hybrid models for weather and climate applications. In T. Brunschwiler et al. (Eds.), *How to use the power of ai to reduce the impact of climate change on switzerland.* Swiss Academy of Engineering Sciences (SATW). Retrieved from https://www.satw.ch/en/publications/how-to-use-the-power-of-ai-to-reduce-the-impact-of-climate-change-on-switzerland

Bevere, L., & Weigel, A. (2021). Sigma: Natural catastrophes in 2020: secondary perils in the spotlight, but don't forget primary-peril risks. *Swiss Re Institute*, *1*. Retrieved from https://www.swissre.com/dam/jcr:706844c8-31c1-44ad-8e32-0166c93d9466/sigma-1-2021-en.pdf

Bi, K., Xie, L., Zhang, H., Chen, X., Gu, X., & Tian, Q. (2023, July). Accurate medium-range global weather forecasting with 3D neural networks. *Nature*, *619*(7970), 533–538. Retrieved 2024-03-08, from https://www.nature.com/articles/s41586-023-06185-3 (Publisher: Nature Publishing Group) doi: 10.1038/s41586-023-06185-3

Bodnar, C., Bruinsma, W. P., Lucic, A., Stanley, M., Brandstetter, J., Garvan, P., ... Perdikaris, P. (2024). *Aurora: A foundation model of the atmosphere.*

Bonavita, M. (2024). On some limitations of current machine learning weather prediction models. *Geophysical Research Letters*, *51*(12), e2023GL107377. Retrieved from https://agupubs.onlinelibrary.wiley.com/doi/abs/10.1029/2023GL107377 (e2023GL107377 2023GL107377) doi: https://doi.org/10.1029/2023GL107377

Bonev, B., Kurth, T., Hundt, C., Pathak, J., Baust, M., Kashinath, K., & Anandkumar, A. (2023, 23–29 Jul). Spherical Fourier neural operators: Learning stable dynamics on the sphere. In A. Krause, E. Brunskill, K. Cho, B. Engelhardt, S. Sabato, & J. Scarlett (Eds.), *Proceedings of the 40th international conference on machine learning* (Vol. 202, pp. 2806–2823). PMLR. Retrieved from https://proceedings.mlr.press/v202/bonev23a.html

Bouallègue, Z. B., Clare, M. C. A., Magnusson, L., Gascón, E., Maier-Gerber, M., Janoušek, M., ... Pappenberger, F. (2024). The rise of data-driven weather forecasting: A first statistical assessment of machine learning-based weather forecasts in an operational-like context. *Bulletin of the American Meteorological Society*. Retrieved from https://journals.ametsoc.org/view/journals/bams/aop/BAMS-D-23-0162.1/BAMS-D-23-0162.1.xml doi: 10.1175/BAMS-D-23-0162.1

Bougeault, P., Toth, Z., Bishop, C., Brown, B., Burridge, D., Chen, D. H., ... Wor-

ley, S. (2010). The thorpex interactive grand global ensemble. *Bulletin of the American Meteorological Society*, *91*(8), 1059 - 1072. Retrieved from https://journals.ametsoc.org/view/journals/bams/91/8/2010bams2853_1.xml doi: 10.1175/2010BAMS2853.1

Bowen, S., Kerschner, B., & Zheng Ng, J. (2024). Natural catastrophe and climate report 2023. *Gallagher Re*. Retrieved from https://www.ajg.com/gallagherre/-/media/files/gallagher/gallagherre/news-and-insights/2024/january/natural_catastrophe_and_climate_report_2023.pdf

Brooks, H., Marsh, P., Kowaleski, A., Groenemeijer, P., Thompson, T., Schwartz, C., ... Buckey, D. (2011). Evaluation of european storm forecast experiment (estofex) forecasts. *Atmospheric Research*, *100*(4), 538-546. Retrieved from https://www.sciencedirect.com/science/article/pii/S0169809510002425 (5th European Conference on Severe Storms) doi: https://doi.org/10.1016/j.atmosres.2010.09.004

Brooks, H. E. (2013). Severe thunderstorms and climate change. *Atmospheric Research*, *123*, 129–138. Retrieved from 10.1016/j.atmosres.2012.04.002 (Publisher: Elsevier B.V.) doi: 10.1016/j.atmosres.2012.04.002

Brooks, H. E., Lee, J. W., & Craven, J. P. (2003). The spatial distribution of severe thunderstorm and tornado environments from global reanalysis data. *Atmospheric Research*, *67-68*, 73–94. (ISBN: 0169-8095) doi: 10.1016/S0169-8095(03)00045-0

Brunet, G., Parsons, D. B., Ivanov, D., Lee, B., Bauer, P., Bernier, N. B., ... Yu, R. (2023). Advancing weather and climate forecasting for our changing world. *Bulletin of the American Meteorological Society*, *104*(4), E909 - E927. Retrieved from https://journals.ametsoc.org/view/journals/bams/104/4/BAMS-D-21-0262.1.xml doi: 10.1175/BAMS-D-21-0262.1

Charlton-Perez, A. J., Dacre, H. F., Driscoll, S., Gray, S. L., Harvey, B., Harvey, N. J., ... Volonté, A. (2024). Do AI models produce better weather forecasts than physics-based models? A quantitative evaluation case study of Storm Ciarán. *npj Climate and Atmospheric Science*, *7*. doi: 10.1038/s41612-024-00638-w

Chen, L., Zhong, X., Zhang, F., Cheng, Y., Xu, Y., Qi, Y., & Li, H. (2023, November). FuXi: a cascade machine learning forecasting system for 15-day global weather forecast. *npj Climate and Atmospheric Science*, *6*(1), 1–11. Retrieved 2024-04-04, from https://www.nature.com/articles/s41612-023-00512-1 (Publisher: Nature Publishing Group) doi: 10.1038/s41612-023-00512-1

Copernicus Services. (2020). *Surface air temperature for march 2020, accessed on 2024-05-24.* Retrieved from https://climate.copernicus.eu/surface-air-temperature-march-2020

Dean, A., & Dial, G. (2020). *Day 4-8 severe weather outlook issued on apr 8, 2020; accessed on 2024-05-24.* Retrieved from https://www.spc.noaa.gov/products/exper/day4-8/archive/2020/day4-8_20200408.html

Ebert-Uphoff, I., & Hilburn, K. (2023). The outlook for ai weather prediction. *Nature Briefing*. doi: 10.1038/d41586-023-02084-9

ECMWF. (2023). *ai-models; last accessed: 12-12-2023.* Retrieved from https://github.com/ecmwf-lab/ai-models

Gilleland, E. (2013). Testing competing precipitation forecasts accurately and efficiently: The spatial prediction comparison test. *Monthly Weather Review*, *141*(1), 340 - 355. Retrieved from https://journals.ametsoc.org/view/journals/mwre/141/1/mwr-d-12-00155.1.xml doi: 10.1175/MWR-D-12-00155.1

Gilleland, E., Ahijevych, D., Brown, B. G., Casati, B., & Ebert, E. E. (2009). Intercomparison of spatial forecast verification methods. *Weather and Forecasting*, *24*(5), 1416 - 1430. Retrieved from https://journals.ametsoc.org/view/journals/wefo/24/5/2009waf2222269_1.xml doi: 10.1175/2009WAF2222269

.1

Govett, M., Bah, B., Bauer, P., Berod, D., Bouchet, V., Corti, S., ... Williams, K. (2024). Exascale computing and data handling: Challenges and opportunities for weather and climate prediction. *Bulletin of the American Meteorological Society*. Retrieved from https://journals.ametsoc.org/view/journals/bams/aop/BAMS-D-23-0220.1/BAMS-D-23-0220.1.xml doi: 10.1175/BAMS-D-23-0220.1

Haiden, T., Janousek, M., Vitart, F., Ferranti, L., & Prates, F. (2019, 11/2019). *Evaluation of ecmwf forecasts, including the 2019 upgrade* (No. 853). ECMWF. Retrieved from https://www.ecmwf.int/node/19277 doi: 10.21957/mlvapkke

Hakim, G. J., & Masanam, S. (2024). Dynamical tests of a deep-learning weather prediction model. *Artificial Intelligence for the Earth Systems*. Retrieved from https://journals.ametsoc.org/view/journals/aies/aop/AIES-D-23-0090.1/AIES-D-23-0090.1.xml doi: 10.1175/AIES-D-23-0090.1

Hersbach, H., Bell, B., Berrisford, P., Hirahara, S., Horányi, A., Muñoz-Sabater, J., ... Thépaut, J.-N. (2020). The era5 global reanalysis. *Quarterly Journal of the Royal Meteorological Society*, *146*(730), 1999-2049. Retrieved from https://rmets.onlinelibrary.wiley.com/doi/abs/10.1002/qj.3803 doi: https://doi.org/10.1002/qj.3803

Houze, R. A. (2014). Chapter 8 - cumulonimbus and severe storms. In R. A. Houze (Ed.), *Cloud dynamics* (Vol. 104, p. 187-236). Academic Press. Retrieved from https://www.sciencedirect.com/science/article/pii/B9780123742667000081 doi: https://doi.org/10.1016/B978-0-12-374266-7.00008-1

Jeppesen, J. (2024, January). *European met services pool resources to intensify use of AI in weather prediction* [Text]. Retrieved 2024-05-28, from https://www.ecmwf.int/en/about/media-centre/news/2024/european-met-services-pool-resources-intensify-use-ai-weather

Kunz, M. (2007). The skill of convective parameters and indices to predict isolated and severe thunderstorms. *Natural Hazards and Earth System Sciences*, *7*(2), 327–342. Retrieved from https://nhess.copernicus.org/articles/7/327/2007/ doi: 10.5194/nhess-7-327-2007

Ladwig, W. (2017). *wrf-python (version 1.3.4.1) [software].* Retrieved from https://doi.org/10.5065/D6W094P1

Lam, R., Sanchez-Gonzalez, A., Willson, M., Wirnsberger, P., Fortunato, M., Alet, F., ... Battaglia, P. (2023, December). Learning skillful medium-range global weather forecasting. *Science*, *382*(6677), 1416–1421. Retrieved 2024-01-11, from https://www.science.org/doi/full/10.1126/science.adi2336 (Publisher: American Association for the Advancement of Science) doi: 10.1126/science.adi2336

Lang, S., Alexe, M., Chantry, M., Dramsch, J., Pinault, F., Raoult, B., ... Rabier, F. (2024). *Aifs - ecmwf's data-driven forecasting system.*

Lawson, J. R., & Gallus Jr, W. A. (2016). Adapting the sal method to evaluate reflectivity forecasts of summer precipitation in the central united states. *Atmospheric Science Letters*, *17*(10), 524-530. Retrieved from https://rmets.onlinelibrary.wiley.com/doi/abs/10.1002/asl.687 doi: https://doi.org/10.1002/asl.687

Leon, J. A. P. (2018, October). *Addressing biases in near-surface forecasts* [Text]. Retrieved 2024-04-26, from https://www.ecmwf.int/en/newsletter/157/meteorology/addressing-biases-near-surface-forecasts

Lin, J., Bhouri, M. A., Beucler, T., Yu, S., & Pritchard, M. (2024). *Stress-testing the coupled behavior of hybrid physics-machine learning climate simulations on an unseen, warmer climate.*

Markowski, P., & Richardson, Y. (2010). *Mesoscale Meteorology in Midlatitudes.*

Wiley-Blackwell. doi: 10.1002/9780470682104

McGovern, A., Tissot, P., & Bostrom, A. (2024, January). Developing trustworthy AI for weather and climate. *Physics Today*, *77*(1), 26–31. Retrieved 2024-06-25, from https://doi.org/10.1063/PT.3.5379 doi: 10.1063/PT.3.5379

Mensch, C. A. (2021). Impacts of vertical grid resolution on the representation of a convective environment. *ProQuest Dissertations and Theses*, 141. Retrieved from https://www.proquest.com/dissertations-theses/impacts-vertical-grid-resolution-on/docview/2549273827/se-2 (Copyright - Database copyright ProQuest LLC; ProQuest does not claim copyright in the individual underlying works; Zuletzt aktualisiert - 2023-03-08)

Mittermaier, M. P. (2021). A "meta" analysis of the fractions skill score: The limiting case and implications for aggregation. *Monthly Weather Review*, *149*(10), 3491 - 3504. Retrieved from https://journals.ametsoc.org/view/journals/mwre/149/10/MWR-D-18-0106.1.xml doi: 10.1175/MWR-D-18-0106.1

Nguyen, T., Brandstetter, J., Kapoor, A., Gupta, J. K., & Grover, A. (2023, July). *ClimaX: A foundation model for weather and climate.* arXiv. Retrieved 2023-11-15, from http://arxiv.org/abs/2301.10343 (arXiv:2301.10343 [cs]) doi: 10.48550/arXiv.2301.10343

Olivetti, L., & Messori, G. (2024a). Advances and prospects of deep learning for medium-range extreme weather forecasting. *Geoscientific Model Development*, *17*(6), 2347–2358. Retrieved from https://gmd.copernicus.org/articles/17/2347/2024/ doi: 10.5194/gmd-17-2347-2024

Olivetti, L., & Messori, G. (2024b). Do data-driven models beat numerical models in forecasting weather extremes? a comparison of ifs hres, pangu-weather and graphcast. *EGUsphere*, *2024*, 1–35. Retrieved from https://egusphere.copernicus.org/preprints/2024/egusphere-2024-1042/ doi: 10.5194/egusphere-2024-1042

Rasp, S., Hoyer, S., Merose, A., Langmore, I., Battaglia, P., Russel, T., ... Sha, F. (2024). *Weatherbench 2: A benchmark for the next generation of data-driven global weather models.* doi: 10.48550/arXiv.2308.15560

Storm Prediction Center. (2020a). *20200412's storm reports (20200412 1200 utc - 20200413 1159 utc); accessed on 2024-05-28.* Retrieved from https://www.spc.noaa.gov/exper/archive/event.php?date=20200412

Storm Prediction Center. (2020b). *20200413's storm reports (20200413 1200 utc - 20200414 1159 utc); accessed on 2024-05-28.* Retrieved from https://www.spc.noaa.gov/exper/archive/event.php?date=20200413

Taszarek, M., Allen, J. T., Groenemeijer, P., Edwards, R., Brooks, H. E., Chmielewski, V., & Enno, S.-E. (2020, December). Severe Convective Storms across Europe and the United States. Part I: Climatology of Lightning, Large Hail, Severe Wind, and Tornadoes. *Journal of Climate*, *33*(23), 10239–10261. Retrieved 2024-01-29, from https://journals.ametsoc.org/view/journals/clim/33/23/jcliD200345.xml (Publisher: American Meteorological Society Section: Journal of Climate) doi: 10.1175/JCLI-D-20-0345.1

Taszarek, M., Allen, J. T., Marchio, M., & Brooks, H. E. (2021, June). Global climatology and trends in convective environments from ERA5 and rawinsonde data. *npj Climate and Atmospheric Science*, *4*(1), 1–11. Retrieved 2024-01-29, from https://www.nature.com/articles/s41612-021-00190-x (Number: 1 Publisher: Nature Publishing Group) doi: 10.1038/s41612-021-00190-x

Taszarek, M., Brooks, H. E., & Czernecki, B. (2017, April). Sounding-Derived Parameters Associated with Convective Hazards in Europe. *Monthly Weather Review*, *145*(4), 1511–1528. Retrieved 2024-01-29, from https://journals.ametsoc.org/view/journals/mwre/145/4/mwr-d-16-0384.1.xml (Publisher: American Meteorological Society Section: Monthly Weather Review) doi: 10.1175/MWR-D-16-0384.1

Thepaut, J.-N., & Courtier, P. (1991). Four-dimensional variational data assimilation using the adjoint of a multilevel primitive-equation model. *Quarterly Journal of the Royal Meteorological Society*, *117*(502), 1225-1254. Retrieved from https://rmets.onlinelibrary.wiley.com/doi/abs/10.1002/qj.49711750206 doi: https://doi.org/10.1002/qj.49711750206

Trapp, R. J. (2013). *Mesoscale-convective processes in the atmosphere*. Cambridge University Press.

Wang, Z., Franke, J. A., Luo, Z., & Moyer, E. J. (2021). Reanalyses and a high-resolution model fail to capture the "high tail" of cape distributions. *Journal of Climate*, *34*(21), 8699 - 8715. Retrieved from https://journals.ametsoc.org/view/journals/clim/34/21/JCLI-D-20-0278.1.xml doi: 10.1175/JCLI-D-20-0278.1

Wernli, H., Hofmann, C., & Zimmer, M. (2009, December). Spatial Forecast Verification Methods Intercomparison Project: Application of the SAL Technique. *Weather and Forecasting*, *24*(6), 1472–1484. Retrieved 2024-03-27, from https://journals.ametsoc.org/view/journals/wefo/24/6/2009waf2222271_1.xml (Publisher: American Meteorological Society Section: Weather and Forecasting) doi: 10.1175/2009WAF2222271.1

Wernli, H., Paulat, M., Hagen, M., & Frei, C. (2008, November). SAL—A Novel Quality Measure for the Verification of Quantitative Precipitation Forecasts. *Monthly Weather Review*, *136*(11), 4470–4487. Retrieved 2024-04-04, from https://journals.ametsoc.org/view/journals/mwre/136/11/2008mwr2415.1.xml (Publisher: American Meteorological Society Section: Monthly Weather Review) doi: 10.1175/2008MWR2415.1

Wong, C. (2023). Deepmind ai accurately forecasts weather — on a desktop computer. *Nature Briefing*. doi: 10.1038/d41586-023-03552-y

Supporting Information for "Lightning-Fast Convective Outlooks: Predicting Severe Convective Environments with Global AI-based Weather Models"

Monika Feldmann[1], Tom Beucler[2], Milton Gomez[2], Olivia Martius[1]

[1]Institute of Geography - Oeschger Centre for Climate Change Research, University of Bern

[2]Faculty of Geosciences and Environment - Expertise Center for Climate Extremes, University of Lausanne

arXiv:2406.09474v2 [physics.ao-ph] 9 Sep 2024

Contents of this file

1. Text S1: Computation of convective parameters
2. Table S1: Model Information
3. Table S2: Performance Scores
4. Table S3: Convective Regions
5. Table S4: Forecast scores of April 13, 06 UTC, 30h lead-time
6. Table S5: Forecast scores of April 13, 06 UTC, 74 lead-time
7. Figure S1: Comparison of vertical profiles for April 12, 2020, 12 UTC
8. Figure S2: 12 UTC initializations for seasonal scores in the USA

Corresponding author: M. Feldmann (monika.feldmann@unibe.ch)

9. Figure S3: CAPE and DLS forecasts for July 7, 2020, 06 UTC

Introduction

The supporting information presented here contains additional details in the computation of convective parameters, the interpretation of performance scores, an additional case study, and performance scores for the variable WMS.

Text S1: Computation of convective parameters

To compute the most unstable CAPE, the parcel profile is launched at the level of the highest equivalent potential temperature. WRF-python takes the surface temperature, pressure, and altitude as input, in addition to the pressure-level temperature, humidity, and geopotential height. Thus it accounts for the altitude of the surface for parcel profiles. CAPE itself is the integral between the parcel and environmental temperature profiles, where the parcel is buoyant.

$$CAPE = g \cdot \int_{z_{LFC}}^{z_{LNB}} \frac{T_v' - T_v}{T_v}\, dz\,, \tag{1}$$

where T_v is the virtual temperature of the environment, T'_v the virtual temperature of the lifted parcel, g the gravity constant, z the altitude, LFC the level of free convection and LNB the level of neutral buoyancy.

To obtain the DLS, the magnitude of the differential vector between surface and mid-atmospheric winds is computed:

$$DLS = \sqrt{(u_{500} - u_{sfc})^2 + (v_{500} - v_{sfc})^2}\,, \tag{2}$$

where u and v are the horizontal components of wind at the surface and 500 hPa level. The compound parameter WMS combines DLS and CAPE in the following manner:

$$WMS = \sqrt{2 \cdot CAPE} \cdot DLS \tag{3}$$

Table S1: Model information

Table S1 provides an overview of the available pressure levels for each model, their primary moisture variable, and the main training period.

Table S2: Performance Scores

Table S2 summarizes the range of each forecast score, as well as its optimal value. The FSS identifies the area fraction of the target variable exceeding a user-defined threshold. We use an area with a radius of 1° in which the fraction exceeding the threshold is evaluated. A FSS value of 1 indicates a perfect forecast (see Table S2). To interpret the SAL, a negative structure score indicates a too-fine spatial structure and too-small areas; a positive score indicates a too-large and too-flat distribution of values (smoothing). A low amplitude score indicates an underestimation, and a high score an overestimation. The location score accounts for both a mismatch in centroid, as well as a mismatch in overlap. A value of zero in each component indicates are perfect forecast (see Table S2).

Table S3: Convective Regions

Table S3 indicates the area used for each region, as well as the months of their respective convective seasons.

Table S4: Forecast scores of April 12, 12 UTC, 12h lead-time The scores for both Tables S4 and S5 are computed including the sea area, and exclusively in the domain shown in Figs 1 and 2 of the main manuscript.

Table S5: Forecast scores of April 12, 12 UTC, 156h lead-time

Figure S1: Comparison of vertical profiles for April 12, 2020, 12 UTC

Figure S2: 12 UTC initializations for seasonal scores in the USA

Figure S3: CAPE and DLS forecasts for July 7, 2020, 06 UTC

Model	Pressure levels	Moisture variable	Training period
IFS	50, 100, 150, 200, 250, 300, 400, 500, 600, 700, 850, 925, 1000	Q	
ERA5	50, 100, 150, 200, 250, 300, 400, 500, 600, 700, 850, 925, 1000	Q	
Pangu-Weather*	50, 100, 150, 200, 250, 300, 400, 500, 600, 700, 850, 925, 1000	Q	1979-2017
GraphCast*	1, 2, 3, 5, 7, 10, 20, 30, 50, 70, 100, 125, 150, 175, 200, 225, 250, 300, 350, 400, 450, 500, 550, 600, 650, 700, 750, 775, 800, 825, 850, 875, 900, 925, 950, 975, 1000	Q	1979-2017
GraphCast-oper*	50, 100, 150, 200, 250, 300, 400, 500, 600, 700, 850, 925, 1000	Q	1979-2017
FourCastNet*	50, 100, 150, 200, 250, 300, 400, 500, 600, 700, 850, 925, 1000	RH	1979-2015
	Surface variables		
all datasets	2m temperature, 10m wind, mean sea level pressure		

Table S1. Model characteristics, neural weather models marked with an asterisk

Score	Value range	Optimal score
RMSE	≥ 0	0
BIAS	$\pm\infty$	0
FSS	0,1	1
S	-2,2	0
A	-2,2	0
L	0,2	0

Table S2. Forecast evaluation metrics

Region	Latitudes	Longitudes	Months
North America	20/50	250/300	April-August
Europe	35/55	350/30	April-September
Argentina	-40/-25	290/310	September-February
Australia	-35/-20	140/155	September-February

Table S3. Regions

Score	IFS	Pangu-Weather-oper	GraphCast-oper	FourCastNet-oper
		CAPE		
RMSE	312	286	***271**	386
BIAS	-88	90	***1**	-92
FSS_{300}	0.92	0.93	***0.96**	0.93
FSS_{1000}	0.87	***0.91**	*0.88	0.61
S	0.21	0.23	***0.02**	0.27
A	0.18	0.16	***-0.04**	-0.28
L	0.03	***0.02**	0.02	0.03
		DLS		
RMSE	3.3	3.3	***2.9**	3.5
BIAS	0.2	0.2	-0.2	***0.1**
		WMS		
RMSE	332	303	***262**	334
BIAS	88	90	***-24**	-39
FSS_{300}	0.91	0.93	***0.96**	0.92
FSS_{500}	0.91	0.93	***0.95**	0.92
S	*0.31	0.29	0.11	**0.03**
A	0.18	0.18	***-0.06**	-0.09
L	0.03	0.05	***0.02**	*0.03

Table S4. Forecast scores at 12h lead-time, best model is marked in bold and with an asterisk

Score	IFS	Pangu-Weather-oper	GraphCast-oper	FourCastNet-oper
CAPE				
RMSE	829	570	***520**	606
BIAS	-223	210	***60**	-288
FSS_{300}	0.26	0.76	***0.77**	0.51
FSS_{1000}	0.20	0.71	***0.74**	0.36
S	0.54	0.39	***0.17**	0.63
A	-0.69	0.35	***0.09**	-1.06
L	0.34	0.11	***0.09**	0.36
DLS				
RMSE	10.2	***5.1**	5.1	7.7
BIAS	3.2	1.2	***-0.2**	1.2
WMS				
RMSE	870	577	***511**	604
BIAS	-124	216	***39**	-257
FSS_{300}	0.26	0.76	***0.77**	0.51
FSS_{500}	0.26	0.71	***0.74**	0.36
S	0.33	0.51	***0.19**	0.36
A	-0.33	0.40	***0.08**	-0.84
L	0.35	0.11	***0.10**	0.37

Table S5. Same as Table S4 but for 156h lead-time

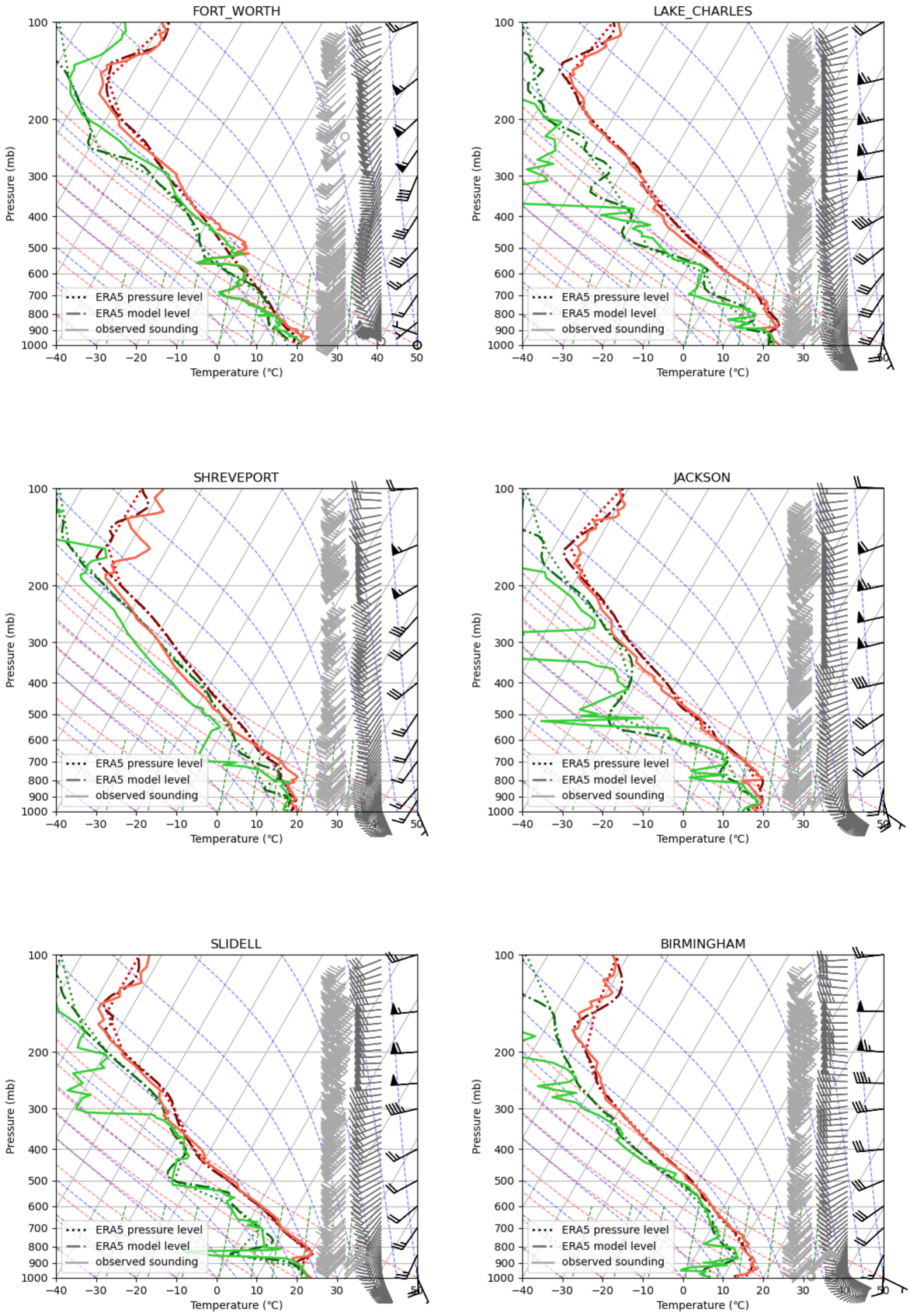


Figure S1. Comparison of soundings from ERA-5 pressure levels, model levels, and measured radiosoundings from 6 locations on April 12, 2020, 12 UTC

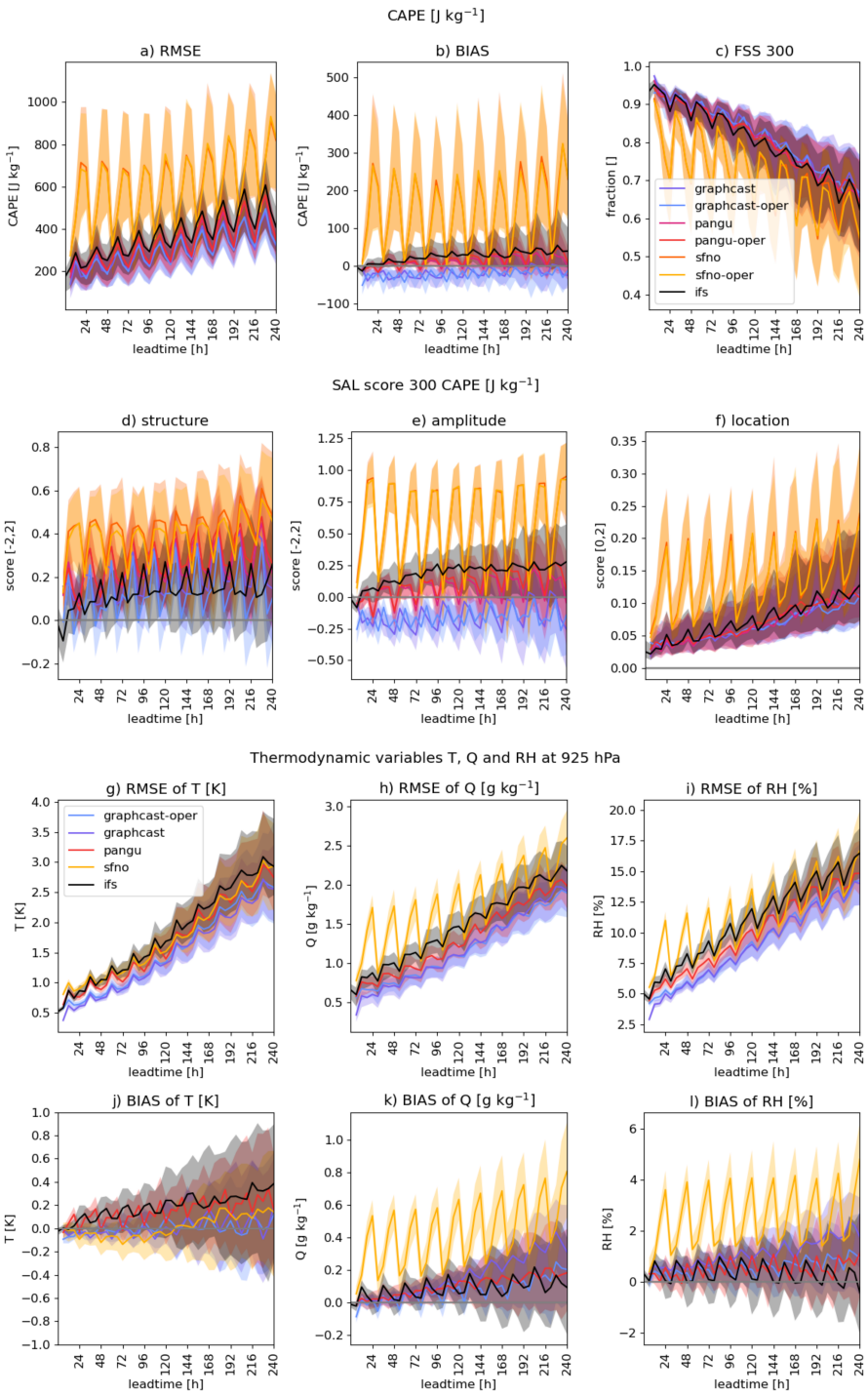


Figure S2. Seasonal evaluation of CAPE for North America at 12 UTC initialization shows Pangu-Weather and GraphCast performing better than IFS, with a moisture bias impacting the performance of FourCastNet. Top row: a) RMSE, b) BIAS, c) FSS_{300}; Second row: SAL components for CAPE >300 J kg^{-1}; color legend in panel c); Third row: RMSE of T, Q and RH at 925 hPa (g-i); Fourth row: BIAS (j-l); model legend in panel g). Solid line depicts the median and shading the interquartile range.

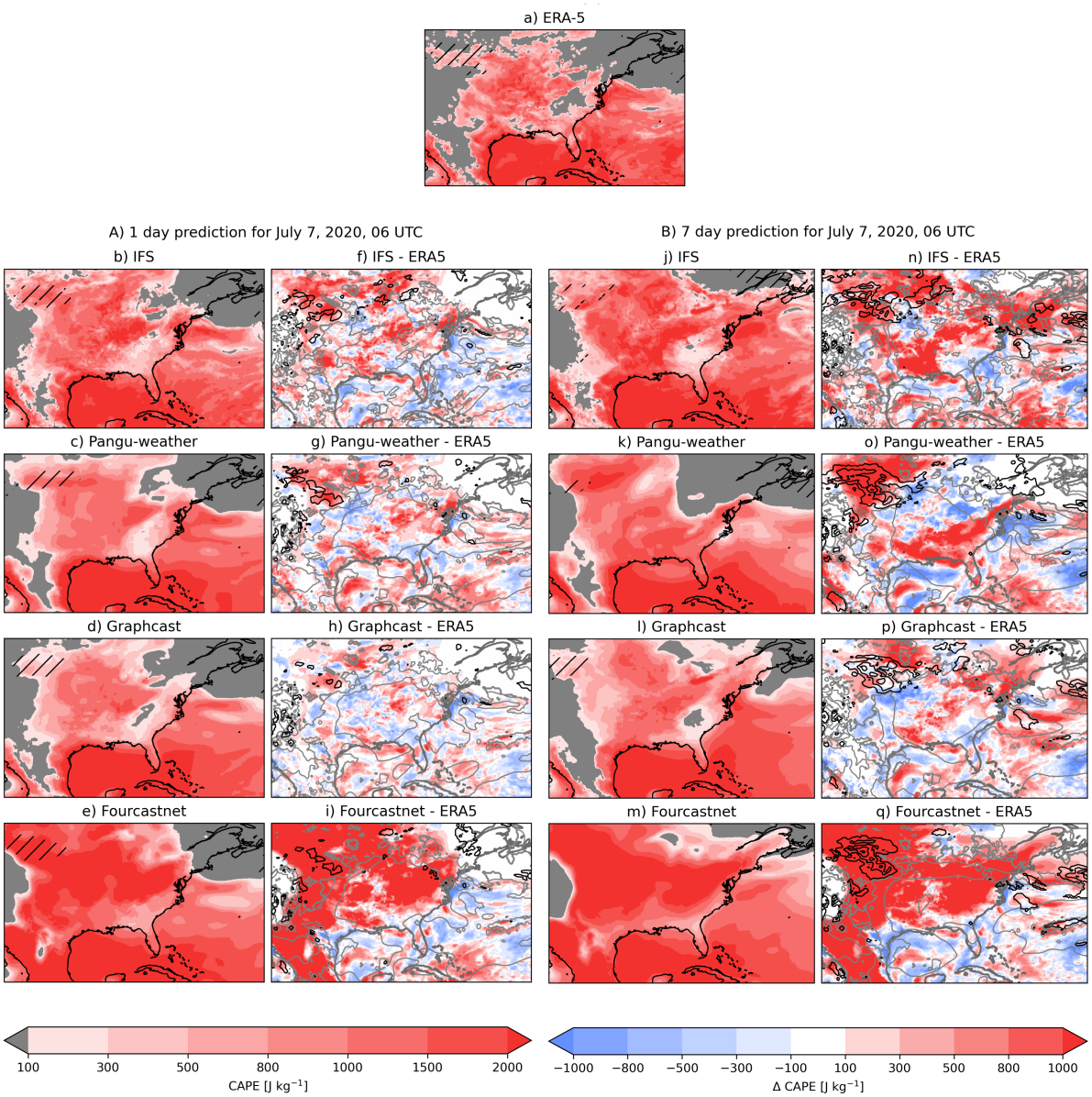


Figure S3. Comparison of forecasts of CAPE and DLS at 1 and 7 days lead-time; a) ERA-5 data of CAPE and DLS on July 7, 2020 at 06 UTC; A) 1 day forecast of CAPE and DLS (b-e) in comparison to ERA5 (f-i) B) 7 day forecast of CAPE and DLS (j-m) in comparison to ERA5 (n-q); hatched area indicates DLS >20 m s^{-1}; contours indicated positive (grey) and negative (black) areas of Δ DLS in 5 m s^{-1} increments